ORIGINAL RESEARCH ARTICLE

Extraction of Nickel from Ultramafic Nickel Sulfide Concentrate by Metallic Iron Addition

FANMAO WANG, SAM MARCUSON, MANQIU XU, MIKE WALKER, and MANSOOR BARATI

Abundant low-grade nickel sulfide ore reserves hold potential as nickel resources but are hindered by high magnesium silicate content, limiting efficient utilization. The authors investigated the possibility of extracting nickel from a low-grade ultramafic nickel sulfide concentrate into ferronickel alloy. The nickel extraction study involved thermal upgrading and physical separation. Thermal upgrading efficiently concentrated nickel values from ultramafic concentrate into ferronickel alloy, achieving over 90 pct extraction with more than 40 pct nickel grade and a characteristic particle size of $d_{80} = 100$ μm. The presence of magnesium silicate gangues in the concentrate adversely impacted the thermal extraction of nickel. Multiple thermal treatment variables have been studied to improve nickel extraction efficiency, including metallic iron addition rate, heating duration, temperature, additives, and atmosphere. The proposed solid-state thermal upgrading method avoided smelting of materials and generation of sulfur dioxide. Magnetic separation recovered approximately 85 pct of nickel in the thermal treatment products into a ferronickel concentrate at 20 pct nickel grade.

https://doi.org/10.1007/s11663-024-03179-y

I. INTRODUCTION

MODERN society demands large quantities of nickel which is widely used in stainless steel, rechargeable batteries, nickel-based alloys, and electroplating.[1,2] Around 30 pct of global nickel output is produced from sulfide nickel ores[3] of which there are two types: high-grade massive nickel sulfide and low-grade disseminated ultramafic. The major nickel-bearing mineral in both types is pentlandite. Ultramafic ores represent a substantial resource base, approximately 11,200 million metric tonnes, primarily found in the USA, Russia, Australia, Canada, China, and Finland.[4] However, they have a low grade, with a nickel content ranging from 0.3 to 1 pct.[4,5] With the depletion of higher-grade sulfide ores and the growing demand for green nickel, processing the abundant ultramafic nickel sulfide ore is mandated.

Ultramafic nickel ores are composed of the minerals pentlandite, pyrrhotite, serpentine, pyroxene, and other magnesium silicates.[6–8] The high magnesium silicate content obstructs pentlandite flotation due to the fibrous nature of this gangue, leading to physical entanglement and an increase in pulp viscosity.[8–10] To enhance separations, various approaches such as mineral surface modifiers,[11–13] fiber disintegration by acid attack,[8] or microwave pre-heating to transform serpentine into olivine[6,7,9] have been explored, but with limited success. Significant levels of Mg still report to concentrate at low nickel grade or recovery. Conventional smelting of the concentrates is limited because high MgO levels produce viscous, high melting point slag. As well, smelting of these concentrates generates sulfur dioxide, which must be captured at significant capital and operating costs. These drawbacks limit commercial utilization of the abundant ultramafic Ni resources.

Recently, sulfation roasting[14] and chlorination roasting[15] followed by water leaching were reported to extract Ni from these low-grade ores. The addition of ammonium sulfate, sodium sulfate, or magnesium chloride aided the extraction of Ni into water-soluble salts. Ni extraction to leachate was 84 to 99 pct, and the maximum Mg extraction was ~ 60 pct.[14,15] In these methods, SO_2 and SO_3 produced during roasting were captured by the additives. Nonetheless, large amounts of additives are needed, leading to potential corrosion issues. Furthermore, successful scale-up necessitates the separation of Ni from Mg and Fe in the leachate.

FANMAO WANG, SAM MARCUSON, and MANSOOR BARATI are with the Department of Materials Science and Engineering, University of Toronto, 184 College Street, Toronto, ON, M5S 3E4, Canada. Contact e-mail: fanmao.wang@mail.utoronto.ca MANQIU XU and MIKE WALKER are with the Vale Base Metals Technology and Innovation, 2060 Flavelle Blvd., Mississauga, ON, L5K 1Z9, Canada.
Manuscript submitted January 3, 2024; accepted June 6, 2024.
Article published online June 24, 2024.

Currently, the high magnesium silicate content in ultramafic nickel concentrate remains a major obstacle for nickel extraction via the pyrometallurgical method. In previous work, the authors demonstrated that it is feasible to extract nickel from high-grade, 18 pct Ni, sulfide concentrates by adding metallic iron, agglomerating the mixture, and treating it in a solid-state thermal upgrading process.[16,17] The reactions proceeded to completion rapidly, residence times of only 100 minutes were required, and thermodynamic calculations reliably predicted product composition and Ni extraction. The products were ferronickel (FeNi), troilite (FeS), and gangue minerals which were separable by magnetic separation. At the process temperature, 1173-1223 K, the formation of molten, viscous slag was avoided and by operating in non-oxidizing conditions, SO_2 emissions were minimized.[17,18] These are significant potential advantages of solid-state nickel extraction.

The authors hypothesized that employing a solid-state nickel extraction method would eliminate the need for smelting ultramafic nickel concentrates, while magnesium silicates would remain inert at low temperatures. Surprisingly, preliminary experiments revealed that Ni was extracted from pentlandite into small FeNi particles ($d_{80} < 50$ μm) with decreasing extraction rates and grades, and the thermodynamic equilibrium was not attained. The causes behind the negative impacts of magnesium silicates on nickel extraction and strategies for enhancing them remain unclear. The proposed nickel extraction method enables nickel to migrate from sulfide phase to metallic ferronickel particles, highlighting the importance of solid-to-solid contact. However, the presence of silicates physically obstructs contact between metallic iron and pentlandite particles. Gangue materials also interact with pentlandite and iron particles, altering the nickel distribution in the product.

The current study explored the reasons behind the subpar performance of thermal upgrading for nickel extraction when large quantities of magnesium silicates are present. It particularly focused on efforts to counteract these negative effects. Variables studied include (1) Fe addition rate, (2) process temperature, (3) effect of additive, and (4) atmosphere composition. Process effectiveness was assessed by (1) nickel extraction to ferronickel (FeNi), (2) nickel grade in FeNi, and (3) FeNi particle size with targets of >90 pct, >30 pct, and d_{80}>100 μm, respectively. Possible chemical reactions and related phenomena are postulated.

II. EXPERIMENTAL

A. *Materials*

Vale Canada provided concentrate. The assay, mineralogy, and microstructure are shown in Table I, Table II, and Figure 1, respectively. The major phases present in the concentrate determined by MLA agree with that examined by XRD analysis, as seen in electronic supplementary Figure S1. Pentlandite was the major Ni-bearing mineral. Pyrrhotite, pyrite, and silicates contained negligible Ni. The elemental compositions of the major minerals were analyzed by electron probe micro-analyzer and are included in an electronic supplementary Table S1. The mass ratio of total sulfides to total silicates and oxides was approximately 2. Silicates had a larger grain size compared to sulfides. The d_{80} of all the mineral particles was around 55 μm by weight. Metallic Fe with >99 pct purity sized 100 pct less than 74 μm was employed as the Ni extractant.

B. *Methods*

1. *Thermodynamic evaluation*

FactSage ™ 7.3[19] was employed to determine the equilibrium composition of mixtures of metallic Fe and concentrate based on process temperature. The databases and solid solutions employed are included in the supplementary material. In the calculations, 100 mass units of normalized Cu–Co–Ni–Fe–S–Mg–Si–O were employed as a basis: Cu 0.42, Co 0.30, Ni 8.99, Fe 36.59, S 25.91, Mg 6.87, Si 6.48, and O 14.44 weight units. These 8 elements accounted for 90.5 mass pct of the ultramafic Ni concentrate. Then, various amounts of metallic Fe were added to the system to evaluate phase evolution and Ni distribution in the final phases. The iron addition rate is expressed by *m*, the mass ratio of Fe addition:concentrate. The authors chose the appropriate metallic Fe addition rate (*m*) for thermal upgrading experiments based on thermodynamic assessment (Section III–A), which illustrates the variations in Ni extraction and grade in FeNi with *m*. When the *m* value falls outside the 0.2 to 0.4 range, the Ni extraction and grade in FeNi become less meaningful in practical terms.

2. *Two-stage thermal treatment*

The two-stage heat treatment process has been described in detail in earlier publications.[16,17] Briefly, mixtures of concentrate + Fe powder + additives (if used) were compacted into briquettes and placed in the hot zone of a horizontal tube furnace at a designated temperature, T1, for a set time, t, under an argon atmosphere. This was the first segment of the two-stage thermal upgrading process. Then, furnace power was reduced to initiate controlled cooling to the specified temperature T2, the second segment of the thermal treatment. When complete, the sample was cooled to room temperature in argon. In various other experiments, the atmosphere consisted of H_2 or CO at temperatures T1 and T2. For safety reasons, the briquettes were initially heated from room temperature to the desired T1 in argon, after which the atmosphere was switched to Ar-H_2 or Ar-CO, as seen in Figure 2(a). Figure 2(b) shows that the briquette integrity was maintained at 1193 K, where incipient melting took place. Table III lists the detailed experimental conditions, including the variables (1) Fe addition rate, (2) thermal treatment duration, (3) experimental temperature, (4) cooling rate, (5) additive parameter, and (6) gas composition.

3. *Comminution and magnetic separation*

A total of 1 kg thermally treated briquettes (Test 17 in Table III) were prepared for separation. A random batch of 600-g briquettes was divided into six groups and then ground to a specific size (100 pct passing 106, 75, and 53 μm). The liberated FeNi particles were then recovered by a handhold magnet in an agitated flotation cell. The applied magnet strength was 250 to 1000 gauss.

C. *Product Analysis*

The chemical compositions of the resulting iron sulfide and silicate phases were determined by electron probe micro-analysis. Mass balances of Ni and Fe in FeNi, iron sulfide, and silicate were employed to calculate both Ni extraction to FeNi and the average Ni grade of FeNi. FeNi grain size was determined by image analysis and was reported as d_{80}, weight basis. The microstructure of the thermal treatment products and magnetic separation products were obtained by scanning electron microscopy. Inductively coupled plasma optical emission spectroscopy was employed to determine chemical assays of the FeNi concentrates and tailings.

III. RESULTS AND DISCUSSION

A. *Thermodynamic Assessment*

The underlying thermodynamics of the process are demonstrated in Figure 3(a), the Fe-rich corner of the Fe–Ni–S phase diagram at 1173 K. The composition of the concentrate normalized to 100 pct Fe–Ni–S is denoted by the red square and lies within the solid iron-nickel sulfide phase domain. As metallic iron is introduced, the normalized composition shifts toward the Fe corner, as indicated by the dashed arrow (Fe addition route). In the process, Ni migrates to the FeNi phase depleting the Ni in sulfide. By adjusting the Fe addition rate one can modify the Ni grade in FeNi and the Ni extraction. Additionally, the removal of S from the system, indicated by the solid arrow, leads to the formation of FeNi, as elaborated upon later in Section III–F.

Prior research has demonstrated that the presence of a small quantity of liquid sulfide is beneficial as it promotes the growth of FeNi particles.[16,17] Figure 3(b) shows that the amount of liquid present was dependent upon both iron addition rate, m, and temperature. To induce incipient melting at $m = 0.25$, the minimum temperature was 1123 K, and at $m = 0.3$-0.5, a temperature of 1173 K or higher was required. The impact of liquid evolution on Ni extraction to FeNi is

Table I. Assay of the As-Received Ultramafic Ni Sulfide Concentrates

Element	Ni	Cu	Co	Fe	S	Mg	Si	Others
Mass Pct	8.1	0.4	0.3	33.1	23.5	6.2	5.9	balance

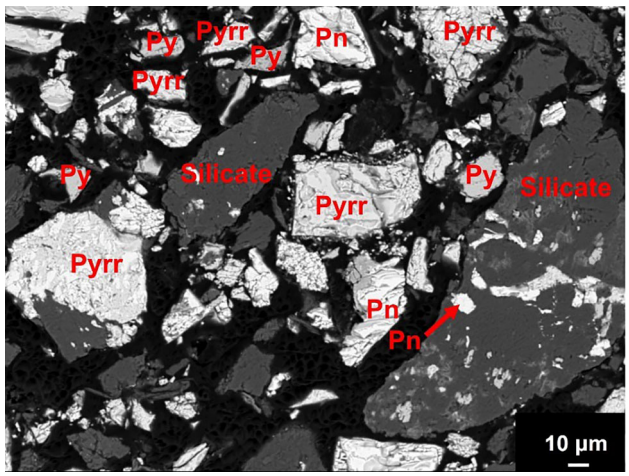

Fig. 1—Microscopic morphology of the as-received ultramafic nickel sulfide concentrate. Pn: pentlandite, Pyrr: pyrrhotite, Py: pyrite, Silicate: serpentine and orthopyroxene.

Table II. Mineralogical Composition Analyzed by Mineral Liberation Analysis (MLA)

Mineral	Chemical Formula	Mass Pct
Pyrrhotite	$Fe_{1-x}S$	33.9
Pentlandite	$(Ni_xFe_y)_9S_8$	20.9
Pyrite	FeS_2	3.4
Violarite	$Fe^{2+}Ni^{3+}{}_2S_4$	1.4
Serpentine	$(Mg, Fe, Al)_3[Si_2O_5](OH)_4$	12.7
Orthopyroxene	$(Mg, Fe, Ca, Al)_2Si_2O_6$	7.9
Talc	$Mg_3Si_4O_{10}(OH)_2$	2.3
Chlorite	$Mg_5Al(AlSi_3O_{10})(OH)_8$	2.3
Amphibole	$\mathbf{AB_2C_5}((Si,Al,Ti)_8O_{22})(OH,F,Cl,O)_2$	1.0
Quartz	SiO_2	0.6
Dolomite	$CaMg(CO_3)_2$	2.8
Magnetite	$Fe^{2+}Fe^{3+}{}_2O_4$	4.3
Iron sulfate	$FeSO_4$	2.5
Total		96.0

A = Ca; **B** = Mg, Fe^{2+}, Ca; **C** = Mg, Fe^{2+}, Co, Ni, Al, Fe^{3+}, Cr^{3+}.

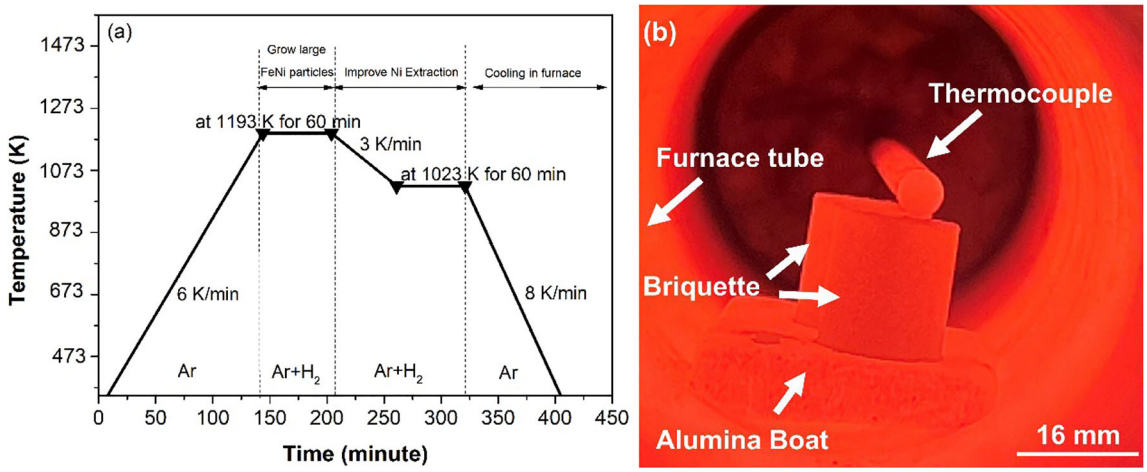

Fig. 2—Two-stage thermal treatment procedure. (*a*) An example under H_2-Ar atmosphere; (*b*) briquettes being heated at 1193 K.

depicted in Figure 3(c). At temperatures above 1223 K, the liquid phase contained more than 80 pct of total Ni value, demonstrating an unacceptable Ni extraction to FeNi alloy. Decreasing the temperature to below 1173 K depleted all the Ni-rich liquid and extracted over 90 pct of Ni into FeNi. The effect of temperature on Ni distribution across different phases shows that an initial treatment at higher temperature, followed by controlled slow cooling and soaking, harnesses both effects effectively, *i.e.*, FeNi particle growth and Ni extraction to FeNi. Figure 3(d) shows the examples of equilibrium Ni extractions and FeNi grades at 1223 K and 1023 K, and the effectiveness of the two-stage process applied to various metallic Fe addition rates, $m = 0.2$-0.6.

B. *Experimental: Effect of Metallic Fe Addition Rate*

Figure 4 compares experimental nickel extractions and FeNi grades with theoretical values over the range $m = 0.2$ to 0.4. As seen, the experimentally determined Ni extraction and grade in the alloy were significantly smaller than the predictions, suggesting that the equilibrium has not been obtained at the established conditions. The discrepancy may be attributed to the presence of large quantities of magnesium silicate in the ultramafic Ni concentrates. Increasing Fe addition rate (m) increased extraction but decreased Ni grade. Maximum Ni extraction was around 85 pct at $m = 0.4$ at a FeNi grade of about 20 pct Ni. Further, the particle size of product FeNi increased with a higher Fe addition rate, and the d_{80} of FeNi particles exceeded 100 μm in all experiments, as seen in Figure S2 in the supplementary material.

Figure 5, micrographs of reaction products, shows that large FeNi particles were the major Ni-bearing phase and had distinct boundaries with the non-metallic phases, FeS, Fe_xO-MgO, and MgO-FeO-SiO_2. The XRD analysis of products from the thermal treatment aligned with the findings from the microstructure analysis (Figure 6). The FexO-rich phase likely originated from the magnetite in the concentrate (approximately 4 mass pct) (Table II) and/or the decomposition of the iron sulfate (2.5 mass pct) initially present. The MgO-FeO-SiO_2 olivine phase contained 20 to 25 pct Fe, comparable to the thermodynamic predictions (24.5 pct Fe), mainly as bivalent iron.[20] By contrast, silicates in the as-received concentrate contained only 2.3 pct Fe, in the form of either bivalent or trivalent iron[20] (Table S1 in the supplementary material). At around 873 K, serpentine begins to decompose as Eq. [1].[20] The high Fe content in the olivine product likely migrated from either the iron sulfides or from the metallic iron addition. Metallic Fe may have reacted with SO_2 released from the iron sulfate [Eq. 2]. In addition, metallic Fe may have reacted with ferric iron in the original serpentine [Eq. 3] and then combined with Mg_2SiO_4 to form MgO-FeO-SiO_2 olivine.

$$2Mg_3Si_2O_5(OH)_4 \rightarrow 3Mg_2SiO_4 + SiO_2 + 4H_2O\ (g), \quad [1]$$

$$\begin{aligned} Fe + 0.5SO_2 \rightarrow FeO + 0.25S_2, \Delta G^{\theta} \\ = -55 \text{ to } -46 \text{ KJ/mol, T} \\ = 973 - 1273 \text{ K}, \end{aligned} \quad [2]$$

$$\begin{aligned} Fe + Fe_2O_3 \rightarrow 3FeO, \Delta G^{\theta} = -37 \text{ to } -54 \text{ KJ/mol, T} \\ = 973 - 1273 \text{ K}. \end{aligned} \quad [3]$$

A typical MgO-FeO-SiO_2 olivine particle had small sulfide grains on its surface, Figures 7(a) and (b). By EPMA point analysis, the olivine analyzed 0.8 pct Ni, larger than that in the original silicate (0.3 pct Ni in **Table S1** in the supplementary material). Studying the development of this microstructure was important to determine whether the surplus Ni came from the Ni-containing small sulfide grains within the silicate or resulted from the dissolution of Ni in the silicate during

Table III. Two-Stage Thermal Upgrading Conditions

Test No.	*m*	Additives (Based on ultramafic concentrate)	Atmosphere During Two-Stage Heating (vol pct)	1st-Stage Temperature (K)	Duration in 1st Stage (min)	Cooling Rate (K/min)	2nd-Stage Temperature (K)	Duration in 2nd Stage (min)
1	0.2		100 pct Ar	1223	30	5	1023	30
2	0.25		100 pct Ar	1223	30	5	1023	30
3	0.3		100 pct Ar	1223	30	5	1023	30
4	0.4		100 pct Ar	1223	30	5	1023	30
5	0.2		100 pct Ar	1223	60	3	973	120
6	0.25		100 pct Ar	1173	30	5	1023	30
7	0.25	5 pct borax	100 pct Ar	1223	30	5	1023	30
8	0.25	5 pct eutectic LiF-NaF	100 pct Ar	1223	30	5	1023	30
9	0.28	5 pct borax, 10 pct FeO	100 pct Ar	1223	30	5	1023	30
10	0.25	10 pct lignite	100 pct Ar	1223	120	5	1023	60
11	0.25		5 pct H_2-95 pct Ar	1223	30	5	1023	30
12	0.25		10 pct H_2-90 pct Ar	1223	30	5	1023	30
13	0.25		20 pct H_2-80 pct Ar	1223	30	5	1023	30
14	0.25		10 pct H_2-90 pct Ar	1223	60	5	1023	60
15	0.25		20 pct H_2-80 pct Ar	1223	60	5	1023	60
16	0.25		5 pct H_2-95 pct Ar	1193	60	3	1023	60
17	0.25		10 pct H_2-90 pct Ar	1193	60	3	1023	60
18	0.25		20 pct H_2-80 pct Ar	1193	60	3	1023	60
19	0.25		20 pct CO-80 pct Ar	1193	60	3	1023	60
20	0.25		20 pct H_2-80 pct Ar *	1193	60	3	1023	60

m is the mass ratio of metallic Fe addition to Ni Concentrate. *The mixed gas was saturated with moisture to simulate reforming gas from natural gas.

the treatment. Elemental mapping shows that Ni primarily coexisted with S rather than Mg or Si, suggesting that this Ni was present in the sulfide form (*i.e.*, small sulfide inclusions) rather than in the silicate phase.

The presence of small sulfides on the MgO-FeO-SiO_2 silicate surface implies that the EPMA point analysis inevitably examined both sulfide and silicate components. A scan of a limited area of the MgO-FeO-SiO_2 silicate grain (Figure 7(b)) determined that the total Ni content within that area was 0.99 pct. Image analysis was employed to map S and Si, revealing a ratio of (area of sulfide)/(area of silicate) = 38.3: 61.7; this area ratio was converted to a mass ratio based on their respective specific gravities, giving s mass of sulfide/mass of silicate = 42.9:57.1. Ni content in pure sulfide was 2.0 pct by EPMA. A Ni mass balance as follows yielded the dissolved Ni in silicate.

$$\text{Total Ni} = \text{Ni content in pure sulfide mass fraction of sulfide grains} + \text{Ni content in silicate mass fraction of silicate.} \quad [4]$$

Around 0.3 pct of Ni was dissolved in the MgO-FeO-SiO_2 silicate, comparable to that in the original silicates of the ultramafic Ni concentrate (Table S1), suggesting a negligible amount of Ni migration from pentlandite to the MgO-FeO-SiO_2 during thermal upgrading. The relatively high reported Ni content in this silicate (Figure 7(b)) was believed to be associated with the sulfide coating rather than the Ni dissolution. Furthermore, the thermodynamic analysis showed that the solubility of Ni in olivine was less than 0.03%. Therefore, the possible distribution of Ni to silicates is discounted.

C. *Effect of Time and Temperature*

The actual Ni extraction at 1023 K with $m = 0.2$ was 78 pct (Figure 4), lower than the thermodynamic prediction of 81 pct, suggesting that the thermal upgrading process did not reach equilibrium. Tests 1 and 5 in Table IV show that increasing the residence time by 2 or 4 times in each stage of treatment neither improved Ni extraction nor increased FeNi particle size. To increase the thermodynamic driving force, the second-stage temperature was lowered from 1023 to 973 K, and residence time increased from 30 to 120 minutes to compensate for slower Ni diffusion. Ni extraction did not improve.

Temperature impacts both the fraction of liquid in the system and the equilibrium distribution of Ni in FeNi. Tests 2 and 6 in Table IV show that decreasing the first-stage temperature from 1223 K to 1173 K increased Ni extraction up to 90 pct. However, the FeNi particle size was reduced due to a smaller amount of liquid at 1173 K. The thermodynamic assessment in Figure 3(b) shows that the liquid fractions at 1223 K and 1173 K were 68 and 5 pct, respectively. In addition, the Ni solubility in the liquid at 1223 K and 1173 K were 10 and 21 pct, respectively.

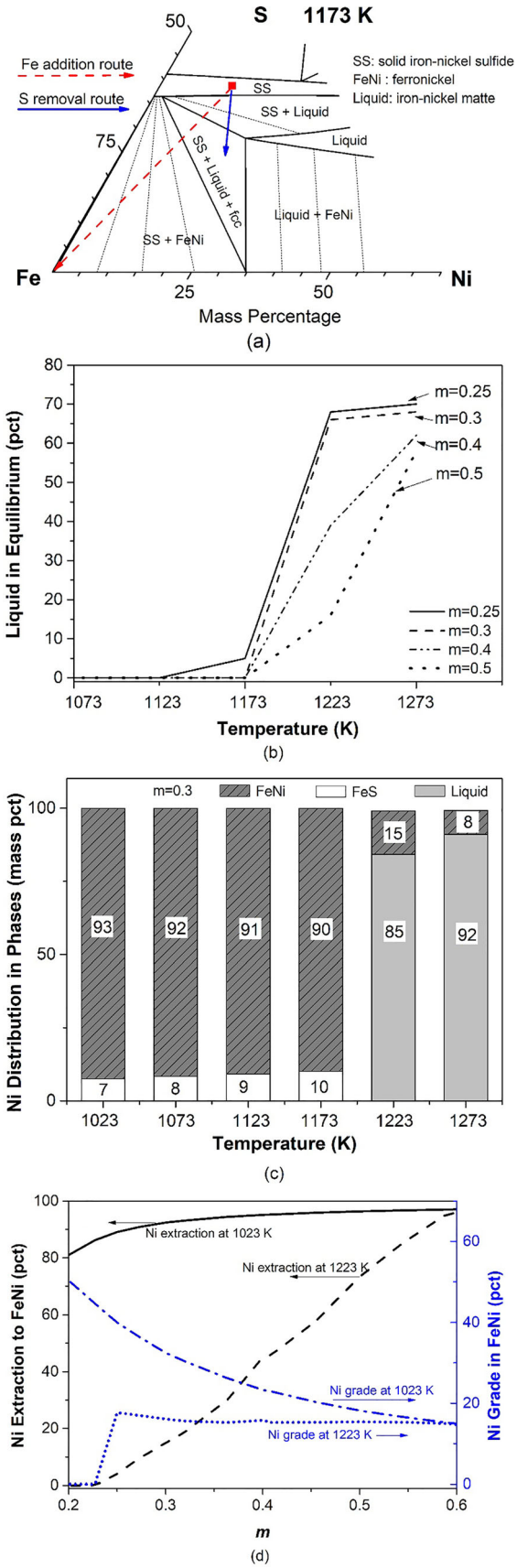

◀Fig. 3—(*a*) Fe–Ni–S phase diagram at 1173 K, (*b*) amount of liquid in the equilibrium versus temperature, (*c*) Ni distribution in multiple phases versus temperature at $m = 0.3$, (*d*) Ni extraction and grade at 1023 K and 1223 K. m = mass of metallic Fe added/mass of concentrate.

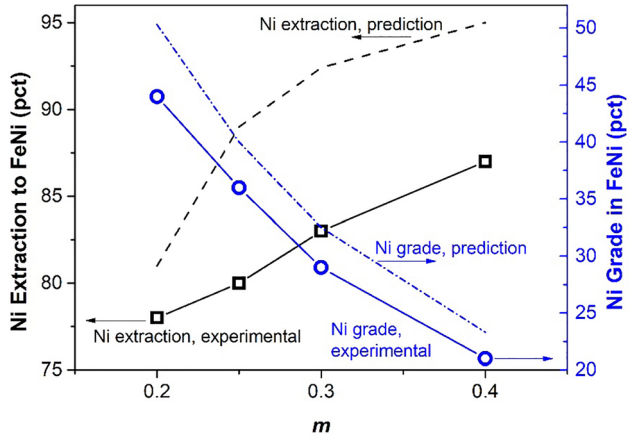

Fig. 4—Ni extraction and grade in product FeNi after two-stage thermal upgrading at 1223 K to 1023 K.

The reduced amount of liquid phase and the lesser distribution of Ni in the liquid at lower temperatures are probable reasons for the improved extraction. It seems that when the first stage of heat treatment generated a significant amount of liquid, the current cooling regime did not retrieve all the Ni from the liquid.

D. *Effect of Silicate-Modifying Additives*

Most likely, the presence of substantial amounts of silicate impeded contact between sulfides and metallic Fe, thereby reducing Ni extraction. To improve sulfide/metallic Fe contact, borate and fluoride fluxing compounds were added to break the silicate structure, Figures 8(a) and (b). As indicated by the smooth interface between sulfides and silicates, melting of the gangue was achieved. The product silicate analyzed 0.02 to 0.03 pct Ni and 0.01 to 0.03 pct S, and the sulfide contained around 2 pct Ni, while the alloy phase contained a Ni content of 31 to 36 pct. Large FeNi grains were formed, but the Ni extraction to FeNi remained less than 85 pct.

After these treatments, the olivine product still contained 20 to 25 pct Fe and it appeared that metallic iron was being "lost" to olivine. To saturate olivine with iron before thermal treatment, 10 pct FeO was added to the concentrate and the mixture was pre-calcined at 1073 K before thermal extraction. Sodium borate was added as flux. Figure 8(c) shows that large FeNi grains were formed. EPMA point analysis reported 1.4 to 1.9 pct Ni in the sulfides. The average Ni grade in FeNi alloy was 20 to 30 pct. In a further effort to reduce Fe distribution to olivine or oxide, lignite was added as a reductant. Figure 8(d) shows that MgO-FeO-SiO_2 olivine remained despite the formation of large FeNi

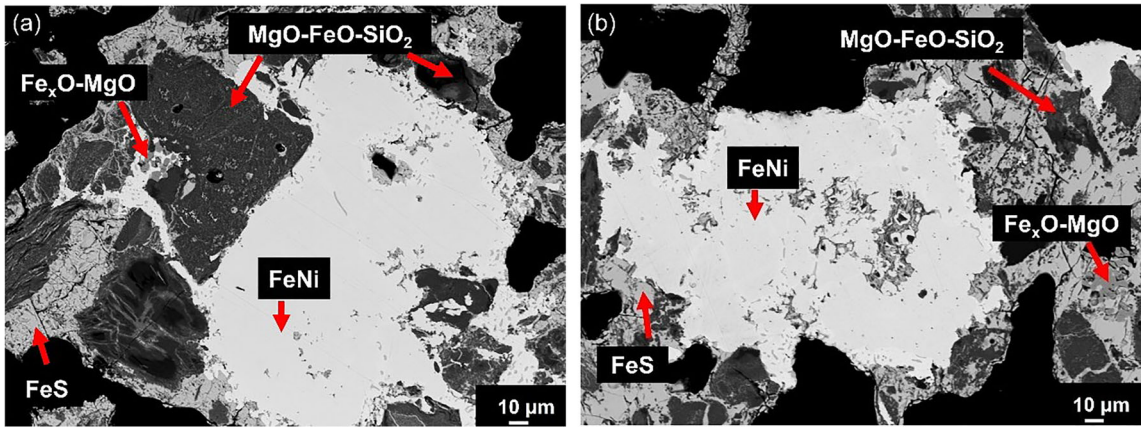

Fig. 5—BSE images of thermal treatment products: (*a*) $m = 0.2$, (*b*) $m = 0.3$. Tests 1 and 3 in Table III. m = amount of metallic Fe/amount of concentrate.

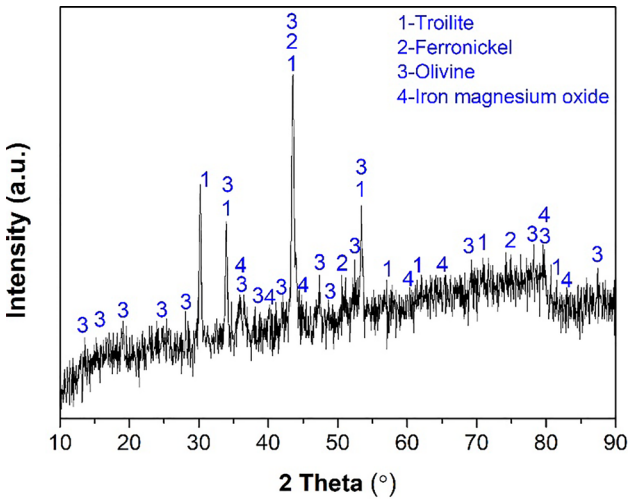

Fig. 6—XRD patterns of thermal treatment products. Test 3 in Table III.

particles. In all tests with silicate-modifying additives, Ni extraction was in the 80 to 85 pct range, and Ni grade varied from 26 to 36 pct. Although the additives aided in separating sulfides and metallics from silicates, their impact on extraction was limited and fell well below the target of 90 pct or higher.

E. *Effect of Atmosphere*

Earlier studies report that S release from the Fe-Ni-S system (e.g., nickeliferous pyrrhotite tailings and high-grade pentlandite concentrates) results in the formation of FeNi particles.[21–23] Further, extensive literature reports the production of metal from metal sulfide by H_2 reduction.[24–26] Therefore, the effect of 5-20 vol pct H_2 in the atmosphere on nickel extraction was studied. Figure 9(a) shows that Ni extraction increases to a maximum at 10 vol pct H_2 and then levels off. At 1223-1023 K, when the atmosphere was changed from 100 pct Ar to 90 pct Ar-10 pct H_2, the Ni extraction reached 88 pct (rectangle symbols), an improvement of 10 pct. By employing a slightly lower temperature, extraction increased further to 91 pct (circle symbols). Further, a longer heating time appears to not improve the Ni extraction. Figure 9(b) shows that any relationship between H_2 concentration and FeNi particle size is weak under the conditions of the present study. FeNi particles with a characteristic size of d_{80}>100 μm were produced in the presence of H_2.

To simulate H_2 produced from natural gas through steam reforming, one experiment (Test 20 in Table III) involved saturating the H_2-Ar gas with moisture. It was found that moisture addition decreased Ni extraction from 91 to 89 pct, suggesting a negative effect of moisture addition. Replacing H_2 with CO (Test 19 in Table III) yielded comparable Ni extraction and FeNi grades; however, the particle size of FeNi decreased to d_{80} = 65 μm.

Three possible explanations may be presented for the favorable effect of a reducing atmosphere on Ni extraction. First, Ni diffusivity in metallic Fe is significantly promoted under H_2. At 973 K to 1273 K, the diffusivity of Ni in Fe is in the range of 5×10^{-11} to 1×10^{-9} cm^2/s under H_2 versus 1×10^{-13} to 1×10^{-11} cm^2/s under N_2,[27] a 10- to 100-fold increase. This narrows the gap between Ni migration in metallic iron and iron sulfide (*i.e.*, 2×10^{-8} to 1×10^{-7} cm^2/s at 973 K to 1273 K[28,29]). Faster mass transport of Ni in Fe promotes Ni extraction and facilitates FeNi particle growth.

Second, H_2 reduction of sulfide lowers the sulfide liquidus temperature, allowing the formation of liquid at a reduced temperature. This facilitates faster Ni transport to FeNi and promotes FeNi growth. It has been reported that H_2 reduces the liquidus temperature of pentlandite from 1118 K to around 1073 K because the decomposed phase $(Ni, Fe)_{3\pm x}S$ contained a higher metal-to-sulfur ratio.[24] It should be noted that, as shown in Figure 3(a), excessive S removal by H_2 can reduce the liquid fraction by shifting the equilibrium from a two-phase region to a three-phase domain. This adverse influence, however, was proved to be limited according to thermodynamic evaluations. The minimum fraction of liquid in equilibrium was calculated based on the determined 7 pct S loss from briquettes experienced

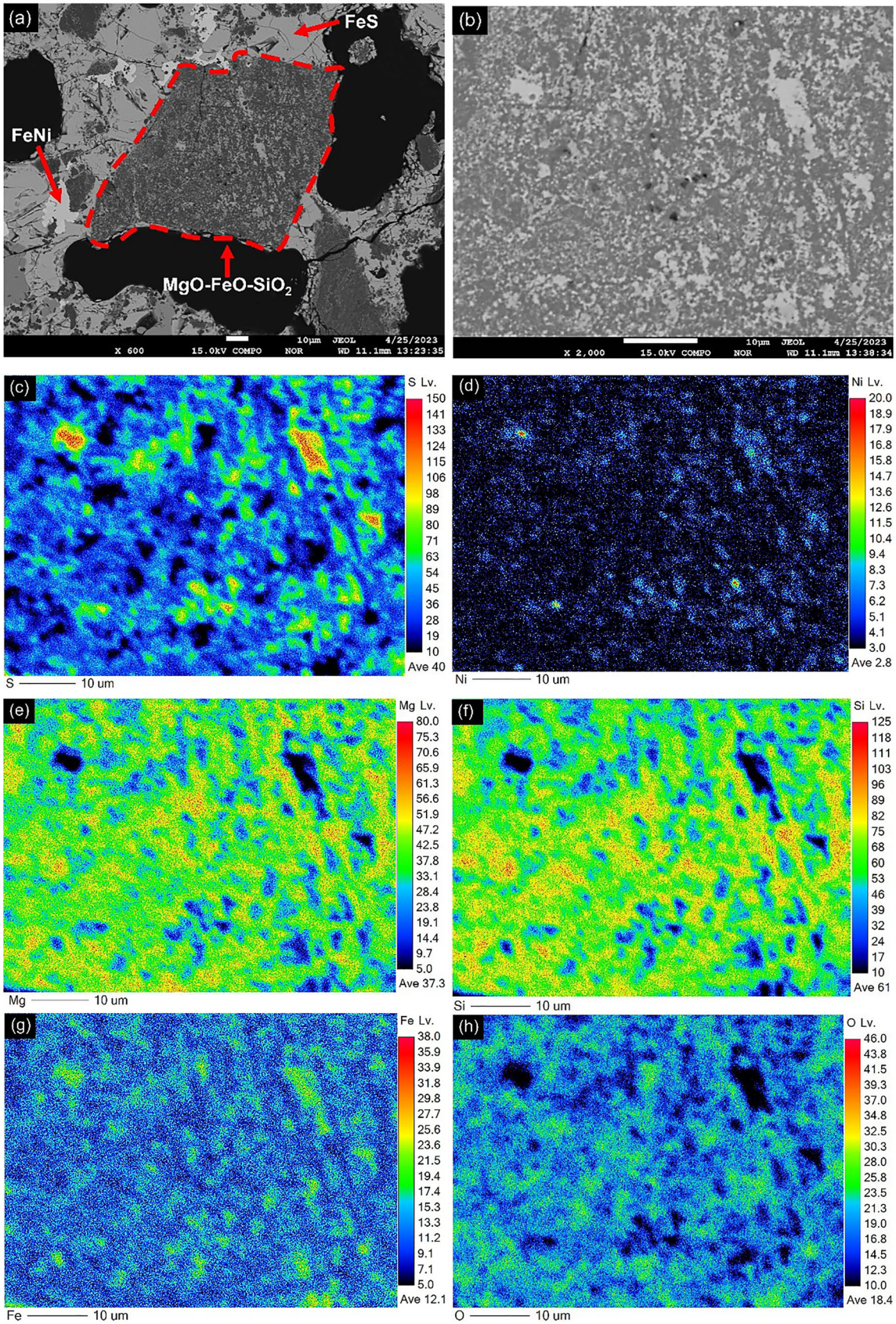

Fig. 7—EPMA mapping of an olivine particle with fine sulfide grains on the surface. (*a*) BSE image at ×600, (*b*) BSE image of the same MgO-FeO-SiO_2 grain at ×2000, the dark matrix was silicate while the light gray was sulfide. EPMA mapping of S (*c*), Ni (*d*), Mg (*e*), Si (*f*), Fe (*g*), and O (*h*). Test 3 in Table III.

Table IV. Effect of Time and Temperature on Ni Extraction

Test No.	m	1st-Stage Temperature (K)	1st-Stage Duration (min)	2nd-Stage Temperature (K)	2nd-Stage Duration (min)	Ni Extraction (Pct)	Ni Grade (Pct)	d_{80} FeNi (μm)
1	0.2	1223	30	1023	30	78	44	130
5	0.2	1223	60	973	120	75	40	113
2	0.25	1223	30	1023	30	80	36	135
6	0.25	1173	30	1023	30	90	45	42

m = Fe addition/concentrate mass.

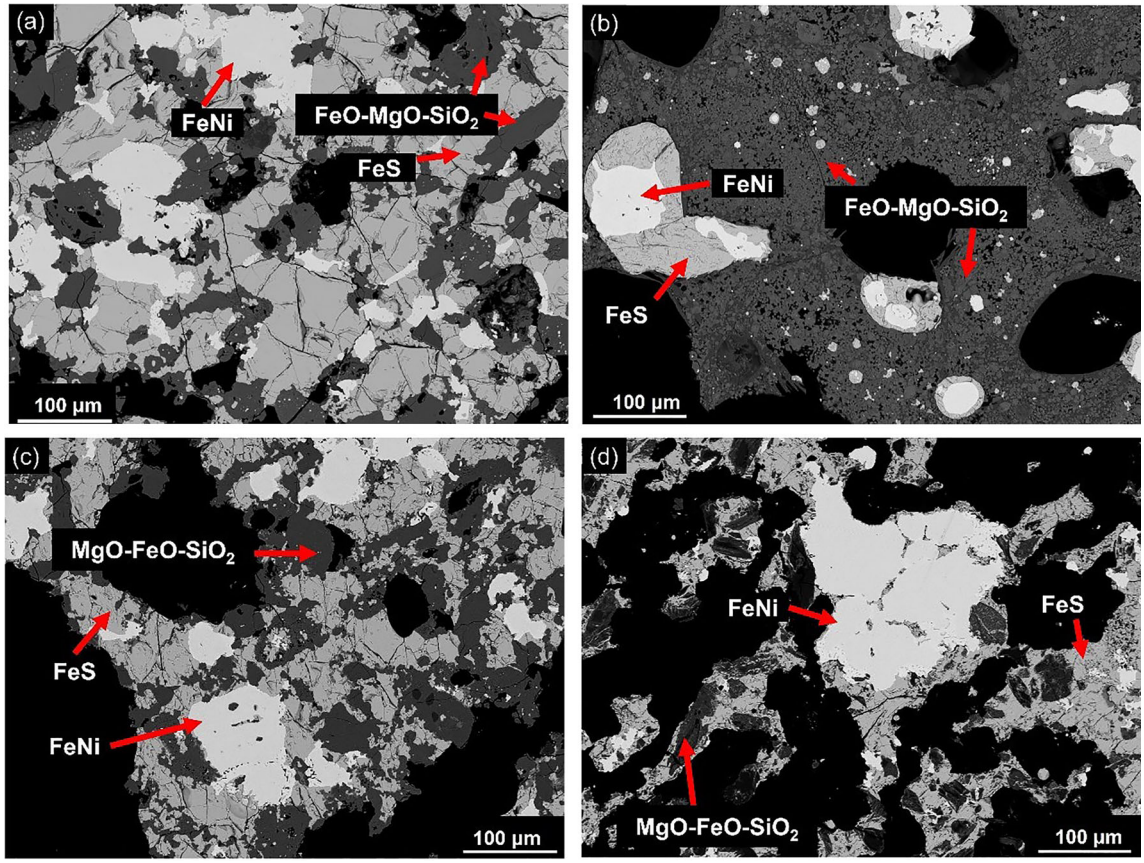

Fig. 8—Thermal treatment products: (*a*) with 5 pct $Na_2B_4O_7$ addition, Test 7 in Table III; (*b*) with 5 pct eutectic LiF-NaF addition, Test 8 in Table III; (*c*) with 10 pct FeO and 5 pct $Na_2B_4O_7$ addition, Test 9 in Table III; (*d*) with 10 pct lignite addition, Test 10 in Table III.

during the thermal treatment. With 10 vol pct H_2 (Test 17 in Table III), the system retained a minimum of 15 pct liquid at 1193 K during the first stage of thermal upgrading. This was still adequate to support the growth of FeNi particles,[17] as evidenced in Figure 9(b).

A third probable reason is that H_2 or CO reduces ferric iron in the serpentine to ferrous iron (Eqs. [5] and [6]) thus mitigating the consumption of metallic iron reagent through Eq. [3]. The excess metallic iron favors a greater extraction of Ni. On the other hand, the further reduction of FeO in MgO-FeO-SiO_2 by H_2 is limited. Literature reports that at P_{H2} = 14 pct and 1170 K, roughly 30 to 40 pct of FeO in the form of fayalite is reduced to metallic Fe.[30] In their research, further reduction is constrained by the presence of MgO, which impedes the diffusion of hydrogen in the product layer.[30] A similar explanation could be relevant to the present study given the substantial MgO content in the MgO-FeO-SiO_2 system.

$$H_2 + Fe_2O_3 \rightarrow 2FeO + H_2O, \quad [5]$$

$$CO + Fe_2O_3 \rightarrow 2FeO + CO_2. \quad [6]$$

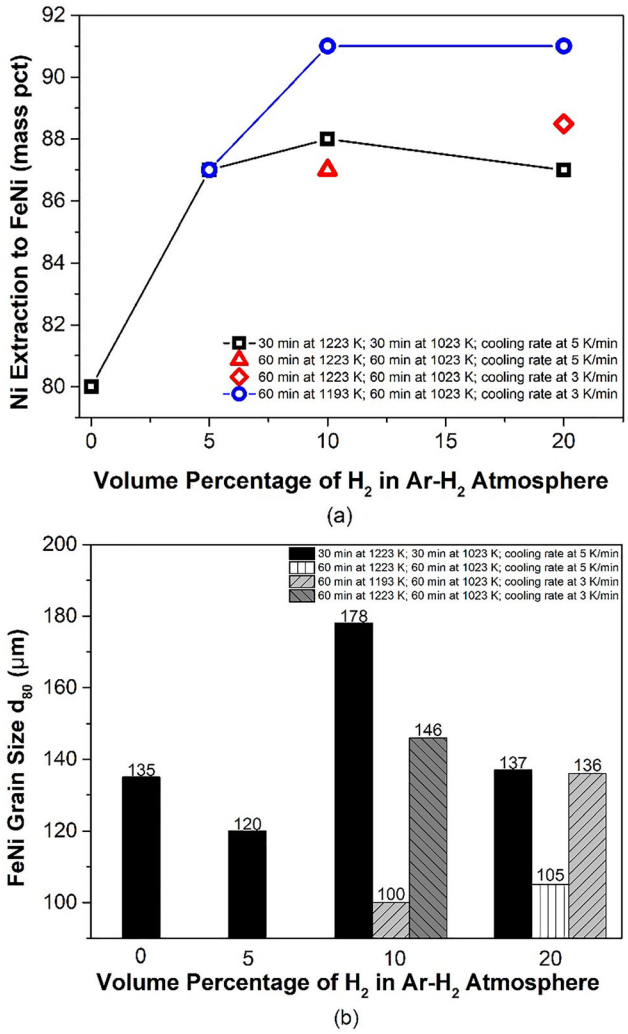

Fig. 9—Effect of H_2 on thermal upgrading: (*a*) Ni extraction to FeNi, (*b*) FeNi grain size. Tests 11 to 18 in Table III.

F. *Recovery of FeNi Grains by Magnetic Separation*

Given that FeNi is highly magnetic, while FeS and olivine are not, magnetic separation proves to be an effective method for recovering the FeNi product. Figure 10(a) plots the cumulative Ni recovery against the cumulative Ni grade for the recovered FeNi concentrate through a laboratory separation. Different grinding sizes and magnetic field strengths have been investigated to separate FeNi from the gangue. It was found that grinding the materials to 100 pct passing 53 μm followed by magnetic separation with 250 gauss recovered 85 pct of Ni recovery into a FeNi concentrate at 20 pct Ni grade. A high-intensity magnetic separation demonstrated limitations in enhancing Ni recovery but significantly reduced Ni grade. Figure 10(b) shows the enrichment of Ni after thermal treatment-magnetic separation. The current research has converted difficult-to-smelt ultramafic concentrate into a FeNi concentrate that can be easily smelted or processed by further means. Improvement in recovery, grade, and impurity content may be achieved by optimization of the combined chemical/physical separation process.

The impurities in the recovered FeNi concentrate came from the remaining FeS and olivine. Highly liberated FeNi particles contained around 4 pct S, 3 pct Mg, and 3 pct Si at 22 pct Ni grade. Partially liberated FeNi materials were analyzed at 10 pct S, 4 pct Mg, and 4 pct Si at 19 pct Ni grade. The non-magnetic tailings, dominated by iron sulfides and silicates, contained only 1.5 pct Ni. The microstructure and assay of the FeNi concentrates and tailings are presented in Figure S3 and Table S2 in the supplementary material. The dendritic morphology and structure of FeNi particles, along with the relatively small alloy size, contribute to the high levels of remaining impurities in the FeNi concentrate. Studies are on the way to promote separation efficiency by growing large FeNi particles with improved morphology – a smoother surface with spherical shape as well as optimization of liberation and separation conditions.

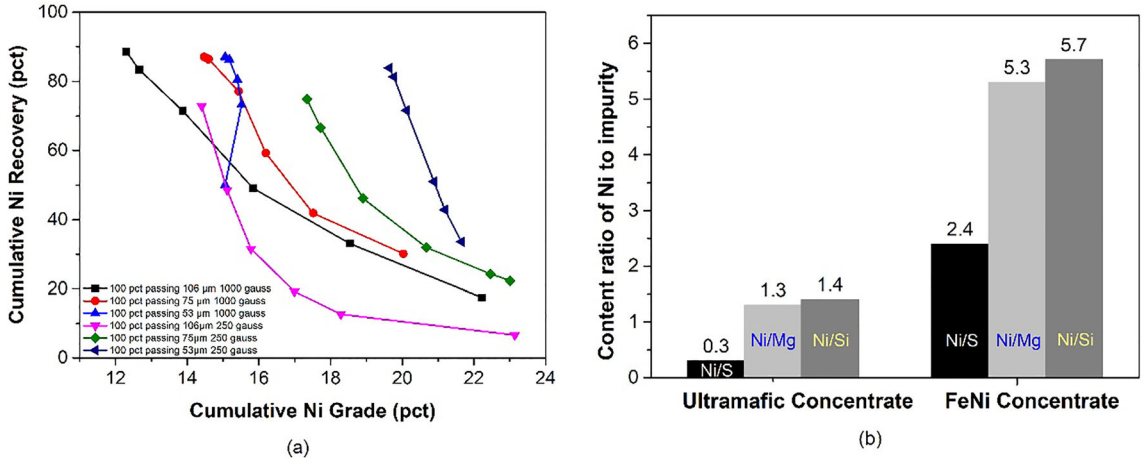

Fig. 10—(*a*) Cumulative Ni recovery versus Ni grade. (*b*) The concentration ratio of Ni to impurities. The 100 pct passing a specific size referred to the grindable materials. The remainder was a non-abrasive alloy and was collected directly as FeNi concentrate without magnetic separation.

IV. CONCLUSION

The current study originated from a concept of solid-state nickel extraction, leveraging its benefit of bypassing smelting of magnesium silicates in low-grade ultramafic nickel concentrate. It then adjusted thermal upgrading parameters to attain high nickel extraction and substantial FeNi particle size. The authors examined the interactions between metallic iron and ultramafic nickel concentrates, nickel distribution within FeNi, iron sulfides, and silicates, as well as the impact of gangue materials on nickel distribution and potential enhancement measures. Conclusions are as follows:

1. The possibility of extracting nickel from an ultramafic Ni concentrate by thermal upgrading was demonstrated. A two-stage process in which metallic iron was mixed with an ultramafic concentrate (Fe/concentrate = 0.4), heated under 100 pct Ar at 1223 K for 30 minutes followed by controlled cooling to 1023 K at 5 K/min and held for 30 minutes achieved a nickel extraction to FeNi of 87 pct at a grade of 20 pct Ni. The d_{80} of the FeNi was 157 μm.
2. The addition of 10-20 vol pct H_2 to the Ar atmosphere facilitated the process, lowering the requisite iron addition by almost 40 pct. The optimum Ni extraction was 91 pct at 42 pct Ni grade in the FeNi and d_{80}(FeNi) = 100 μm.
3. When the products were subjected to low-intensity magnetic separation, the FeNi concentrate analyzed 20 pct Ni at 85 pct Ni recovery. The mass ratios Ni:Mg and Ni:Si were increased from 1 in the original concentrate to 5 in the FeNi product.
4. After solid-state thermal upgrading, the primary phases that formed were FeNi, FeS, MgO-FeO-SiO_2, and Fe_xO-MgO. Certain MgO-FeO-SiO_2 (olivine) grains exhibited minor sulfide deposits on their surfaces. The amount of nickel directly absorbed by olivine was minimal, and most of the nickel in the olivine particles came from the sulfides attached to their surfaces. The introduction of fluxes appeared to reduce the sulfide layer on the surface of olivine.
5. Magnesium silicate in the concentrate hindered reactions by two mechanisms. First, silicates hindered contact between metallic Fe and pentlandite limiting mass transfer. Borate and fluoride fluxes were added but did not improve the effectiveness of the process. Second, by reacting with metallic and/or sulfidic Fe, the silicates ''robbed'' this reagent from productive reactions. The addition of reducing gas ameliorated this phenomenon.

ACKNOWLEDGMENTS

The authors wish to acknowledge the financial support from the Connaught Innovation Fund at the University of Toronto and the Natural Science and Engineering Research Council of Canada (NSERC I2IPJ 566697) and technical support from Vale Canada. Sincere thanks to Dr. Abdolkarim Danaei for his help with the experiments.

CONFLICT OF INTEREST

The authors declare that they have no conflict of interest.

SUPPLEMENTARY INFORMATION

The online version contains supplementary material available at https://doi.org/10.1007/s11663-024-03179-y.

REFERENCES

1. Nickel Institute: About nickel, https://nickelinstitute.org/en/about-nickel-and-its-applications/. Accessed 26 Jun 2023.
2. National Resources Canada: Nickel facts, https://www.nrcan.gc.ca/our-natural-resources/minerals-mining/minerals-metals-facts/nickel-facts/20519. Accessed 26 Jun 2023.
3. A. Vahed, P.J. Mackey, and A.E.M. Warner: *Ni-Co 2021: The 5th International Symposium on Nickel and Cobalt*, C. Anderson, G. Gooddall, S. Gostu, D. Gregurek, and M. Lundström, eds., Springer, New York, NY, 2021, pp. 3–39.
4. M. Xu, K. Scholey, and S. Marcuson: *50th Annual Conference of Metallurgists of CIM*, B.R. Davis and J.P.T. Kapusta, eds., the Canadian Institute of Mining, Metallurgy and Petroleum, Montreal, MTL, 2011, pp. 151–63.
5. S. Khan, M. Shoaib, N. Molaei, O.B. Wani, Z. Chen, T.V. Vuong, E.W. Roth, L.K. Fiddes, I. Kuzmenko, E.R. Master, and E.R. Bobicki: *ACS Sustain. Chem. Eng.*, 2023, vol. 11, pp. 1294–1304.
6. E.R. Bobicki, Q. Liu, and Z. Xu: *Miner. Eng.*, 2014, vol. 58, pp. 22–25.
7. J. Forster, R. Elliott, D. Boucher, and E.R. Bobicki: *Miner. Eng.*, 2021, vol. 172, 107109.
8. S. Uddin, S.R. Rao, M. Mirnezami, and J.A. Finch: *Int. J. Miner. Process.*, 2012, vol. 102–103, pp. 38–44.
9. E.R. Bobicki, Q. Liu, and Z. Xu: *Minerals*, 2018, vol. 8, pp. 1–9.
10. D. Yang, L. Xie, E. Bobicki, Z. Xu, Q. Liu, and H. Zeng: *Langmuir*, 2014, vol. 30, pp. 10809–17.
11. O.B. Wani, S. Manzoor, N. Molaei, M. Shoaib, S. Khan, H. Zeng, and E.R. Bobicki: *Resour. Conserv. Recycl.*, 2022, vol. 186, p. 106496.
12. O.B. Wani, S. Khan, M. Shoaib, H. Zeng, and E.R. Bobicki: *Chem. Eng. J.*, 2022, vol. 433, 134203.
13. O.B. Wani, D. Yang, S. Manzoor, M. Shoaib, S. Khan, H. Zhang, H. Zeng, B. Klein, and E.R. Bobicki: *J. Environ. Chem. Eng.*, 2023, vol. 11, 111213.
14. W. Mu, Z. Huang, H. Xin, S. Luo, Y. Zhai, and Q. Xu: *JOM*, 2019, vol. 71, pp. 4647–58.
15. X. Xu, W. Mu, L. Wang, H. Xin, X. Lei, S. Luo, and Y. Zhai: *JOM*, 2022, vol. 74, pp. 1989–99.
16. F. Wang, S. Marcuson, L.T. Khajavi, and M. Barati: *Metall. Mater. Trans. B*, 2021, vol. 52B, pp. 3120–29.
17. F. Wang, S. Marcuson, M. Xu, and M. Barati: *Metall. Mater. Trans. B*, 2023, vol. 54B, pp. 2758–70.
18. F. Wang, S. Marcuson, L.T. Khajavi, and M. Barati: *Metall. Mater. Trans. B*, 2020, vol. 51B, pp. 2642–52.
19. C.W. Bale, E. Bélisle, P. Chartrand, S.A. Decterov, G. Eriksson, A.E. Gheribi, K. Hack, I. Jung, Y. Kang, J. Melançon, A.D. Pelton, S. Petersen, C. Robelin, J. Sangster, P. Spencer, and M.V. Ende: *Calphad Comput. Coupling Phase Diagrams Thermochem.*, 2016, vol. 54, pp. 35–53.
20. W.A. Deer, R.A. Howie, and J. Zussman: *An Introduction to the Rock-Forming Minerals*, 3rd ed. Mineralogical Society of Great Britain and Ireland, London, LDN, 2013, pp. 4–220.
21. R. Sridhar, A. Dalvi, H.F. Bakker, and A. Illis: *Can. Metall. Q.*, 1976, vol. 15, pp. 255–62.
22. F. Liu, D. Yu, S. Marcuson, F. Wang, B. Li, and M. Barati: *Miner. Eng.*, 2019, vol. 134, pp. 206–14.

23. F. Wang, S. Marcuson, L.T. Khajavi, and M. Barati: *Metall. Mater. Trans. B*, 2021, vol. 52B, pp. 3920–29.
24. I.D. Shah and P.L. Ruzzi: *Metall. Trans. B*, 1978, vol. 9B, pp. 247–53.
25. F. Habashi and R. Dugdale: *Metall. Trans.*, 1973, vol. 4, pp. 1865–71.
26. R. Pathak, T.R. Mankhand, J.S. Kachhawaha, and P.M. Prasad: *Miner. Process. Extr. Metall. Rev.*, 1992, vol. 10, pp. 109–20.
27. F. Liu: Thermal Upgrading of Nickeliferous Pyrrhotite Tailings for Nickel Recovery, University of Toronto, 2021.
28. D.S. Lauretta: *Oxid. Met.*, 2005, vol. 64, pp. 1–22.
29. R.H. Condit, R.R. Hobbins, and C.E. Birchenall: *Oxid. Met.*, 1974, vol. 8, pp. 409–55.
30. C.C. Massieon, A.H. Cutler, and F. Shadmanv: *Ind. Eng. Chem. Res.*, 1993, vol. 32, pp. 1239–44.